Wave packet study of the Ar–HBr photolysis: Stereodynamical effects

R. Prosmiti and A. García-Vela[a)]
Instituto de Matemáticas y Física Fundamental, C.S.I.C., Serrano 123, 28006 Madrid, Spain

(Received 1 July 2002; accepted 12 February 2003)

The ultraviolet photolysis of Ar–HBr($v=1$) is studied through wave packet dynamics simulations, focusing on the fragmentation pathway Ar–HBr $+\hbar\omega \rightarrow$ H+ Ar–Br. Photolysis starts from two initial states of Ar–HBr($v=1$) with a different angular shape, namely the ground and the first excited van der Waals (vdW) states, corresponding to the Ar–H–Br and Ar–Br–H isomers, respectively. It is found that the yield of Ar–Br radical products is substantially higher for the initial excited vdW state of the cluster, where H dissociation is less hindered. In addition, the yield of radical formation is much higher in the Ar–HBr($v=1$) photolysis than that previously found in the Ar–HCl($v=0$) case, even for the ground vdW state, where the initial angular distribution of both clusters is similar. Another unexpected difference is that Ar–HCl($v=0$) photolysis exhibits strong manifestations of quantum interference, while these effects are much weaker in Ar–HBr($v=1$). A lower probability of the first collision between the recoiling hydrogen and the Ar atom in the case of Ar–HBr($v=1$), due to geometrical differences between its initial state and that of Ar–HCl($v=0$), is suggested to explain the different photolysis behavior of both clusters. The implications of the present findings in the photolysis of other related precursor clusters are discussed. © *2003 American Institute of Physics.* [DOI: 10.1063/1.1565312]

I. INTRODUCTION

In the last years there has been a growing interest in the study of the ultraviolet (UV) photolysis of hydrogen-bonded clusters.[1–16] One of the main motivations of such interest is the possibility of preparing highly excited, weakly bound radical complexes, upon ejection of the hydrogen atom after UV photoexcitation of a closed-shell hydrogen-bonded precursor cluster. The highly excited radicals produced allow one to probe the open-shell interactions involved, not only in the region of the potential well, but also in the short- and long-range regions.

Experimental evidence of formation of radical complexes like Ar–I, H–IH, H–ClH, and Ar_n–HS ($n\leqslant 2$) has been found upon UV photolysis of the precursors Ar–HI,[2] $(HI)_2$,[3] $(HCl)_2$,[4] and Ar_n–H_2S ($n\leqslant 2$),[8] respectively. The photolysis experiments on Ar_n–H_2S ($n\leqslant 2$) were carried out at two different excitation wavelengths, namely 193 and 248 nm, for which yields of 1.5% and 15% of Ar–HS radical formation were obtained, respectively. Such yields of radical survival can be considered high, taking into account that the amount of energy released in the photolysis process is much larger than the binding energy of the radical. Formation of Ar–Cl and Ar_n–HS ($n\leqslant 2$) radicals following UV photodissociation of the Ar–HCl[17–19] and Ar_n–H_2S ($n\leqslant 2$)[20] parent clusters, respectively, has also been predicted theoretically.

The mechanism of Ar–Cl formation, Ar–HCl $+\hbar\omega \rightarrow$ H + Ar–Cl (called partial fragmentation pathway), was analyzed in detail by simulating the Ar–HCl($v=0$) photolysis through an exact wave packet method.[18,19] Energy-resolved product fragment distributions were calculated at different excitation energies in the range of the absorption spectrum of the parent cluster. The yield of Ar–Cl formation was found to be very high for low excitation energies of Ar–HCl, corresponding to a range of excess energy deposited in the system of 1 eV$<E<$2 eV. In this range (which is associated with the low probability tail of the absorption spectrum) the Ar–Cl yield decreased sharply from ~80% to ~3%. For excess energies $E>2$ eV the yield kept decreasing slowly, though remaining about 1% for most of the energies in this range.

It was found that as the excess energy of the parent cluster increases (and therefore the amount of energy available for the radical fragment increases as well), the Ar–Cl radicals were produced not only in bound rovibrational states, but also in highly excited quasibound states. These quasibound states (above the Ar–Cl dissociation energy limit) are supported by rotational barriers and associated with a high rotational excitation of the radical fragment. Actually, a similar result was obtained in classical trajectory simulations of the Ar_n–H_2S ($n\leqslant 2$) photolysis,[20] where the Ar_n–HS ($n\leqslant 2$) radicals were produced in the same type of quasibound states with a high probability. Population of these highly excited quasibound states makes possible that the radical accommodates a larger amount of the energy available, which would contribute to enhance its survival probability. It was also found that formation of Ar–Cl was influenced to a large extent by quantum interference effects between the two possible cluster fragmentation pathways, namely partial fragmentation (PF) leading to Ar–Cl and total fragmentation (TF) into H + Ar+Cl.[19]

The UV photolysis of Ar–HBr($v=1$) has been recently investigated by means of quasiclassical trajectory calculations.[21] The goal of that work was to explore the effect of the initial distribution of intracluster orientations on the photolysis process. Thus, cluster photolysis was simu-

a)Electronic mail: garciavela@imaff.cfmac.csic.es

lated by starting from two different initial states of Ar–HBr ($v=1$), namely the ground and the first excited vdW states (this excited state being the first excitation of the vdW bending mode), which correspond to the Ar–H–Br and Ar–Br–H isomers, respectively. Such states represent different initial situations for hydrogen dissociation, which in the first case is hindered to a large extent by the Ar obstacle, while in the second case it is not. It should be mentioned that for both $v=0$ and $v=1$ vibrational states of HBr, the ground and first excited vdW states correspond to the Ar–H–Br and Ar–Br–H isomers, respectively. The reason to choose $v=1$ (instead of $v=0$ as in Ar–HCl) is that in this case the angular distribution associated with the first excited vdW bending state is somewhat more concentrated around the Ar–Br–H geometry.[22] Then, stereodynamical differences arising from the two initial vdW states of Ar–HBr(v) are expected to be somewhat larger for $v=1$ than for $v=0$.

Product fragment distributions associated with the Ar–HBr PF and TF pathways were obtained at different excitation energies of the precursor cluster for the two initial states. The results showed that indeed there is an effect of the angular shape of the cluster initial state. The yield of Ar–Br radical formation was found to be substantially higher for the initial state corresponding to the Ar–Br–H isomer, where hydrogen ejection is much less hindered. In this case the probability of H/Ar collisions is lower, which increases the survival probability of Ar–Br. Interestingly, even when photolysis started from the ground vdW state of Ar–HBr($v=1$), the radical yield obtained was remarkably high for all the excitation energies studied. This behavior is in sharp contrast with the much lower yield of Ar–Cl formation, despite the fact that the initial angular distribution shape of the ground vdW states of Ar–HCl($v=0$) and Ar–HBr($v=1$) is very similar. This result was attributed[21] mainly to the larger amount of energy available for Ar–Cl than for Ar–Br (at the same excitation energy), due to the different H/Cl and H/Br mass ratios.

In the present work exact wave packet simulations of the UV photolysis of Ar–HBr($v=1$) starting from the above-mentioned initial states are reported. The aim is to assess the validity of the trends and conclusions found in the previous quasiclassical trajectory study,[21] by using a more rigorous dynamical treatment which can describe possible quantum effects. Such effects were found to play an important role in the Ar–HCl photolysis, and might also be relevant in the Ar–HBr photodissociation dynamics.

The paper is organized as follows. In Sec. II the dynamical treatment is briefly described, and in Sec. III the results are presented and discussed. Sec. IV is devoted to conclusions.

II. THE METHOD

A. Potential-energy surfaces and initial state

Photolysis of Ar–HBr takes place upon UV excitation of the HBr chromophore from its ground electronic state $X\,^1\Sigma^+$ to the repulsive excited state $A\,^1\Pi$. This excitation is simulated by a Franck–Condon transition between the two electronic states. The potential-energy surfaces used in the present simulations to represent both the ground and the excited electronic states of Ar–HBr, as well as the Ar–HBr($v=1$) initial state in the $X\,^1\Sigma^+$ surface have been described elsewhere.[21,23] The system is represented in the (r,R,θ) Jacobian coordinates, where r is the H–Br distance, R is the separation between the Ar atom and the center of mass of HBr, and θ is the angle between the vectors **r** and **R**. In the definition adopted here, $\theta=0$ corresponds to the collinear configuration Ar–H–Br.

The angular distributions of the initial Ar–HBr($v=1$) ground and first excited vdW states have been discussed in Ref. 21 (see Fig. 1 of that work). Most of the intensity of the angular distribution of the Ar–HBr($v=1$) ground vdW state is located at low θ angles (corresponding to the Ar–H–Br geometry), and it is very similar in shape to the initial angular distribution of the Ar–HCl($v=0$) ground vdW state. By contrast, the initial angular distribution of the Ar–HBr($v=1$) first excited vdW state concentrates at high angles (around the Ar–Br–H geometry).

Upon UV excitation of the initial state to the excited electronic surface the cluster photolyzes following fragmentation into H+Ar–Br (PF) or into H+Ar+Br (TF). In this work we shall focus on the analysis of the PF pathway, which takes place upon direct dissociation of the H fragment. A quasiclassical analysis of the TF product distributions after Ar–HBr($v=1$) photolysis was reported in Ref. 21.

B. Dynamical treatment

The system wave packet $\Phi(r,R,\theta)$ was propagated in the upper electronic surface $A\,^1\Pi$ up to $t_f=80$ fs with a time step $\Delta t=2$ fs. At this final time practically all the wave packet intensity has reached the asymptotic region. Propagation of the wave packet was carried out using the Chebychev polynomial expansion method[24] to represent the time-evolution operator $\exp(-i\hat{H}\Delta t)$. The wave packet was represented on a rectangular grid of 480×270 equally spaced points in the r and R coordinates, respectively, in the ranges 1.6 a.u.$\leqslant r\leqslant$ 52.5 a.u. and 5.6 a.u.$\leqslant R\leqslant$13.7 a.u. A grid of 180 points corresponding to a Gauss–Legendre quadrature was used to represent the angular coordinate in the range $0°\leqslant\theta\leqslant180°$. The above three-dimensional grid defines a discrete variable representation (DVR) where the potential-energy terms of the Hamiltonian were represented. The operations of these terms on the wave packet were evaluated by simple multiplication point by point. The operations of the kinetic-energy terms were evaluated using fast Fourier transform (FFT) techniques in the case of the radial coordinates, and a combination of the above angular DVR and a Legendre polynomial finite basis representation (FBR) in the case of the angular coordinate.[25]

In order to obtain product fragment distributions, the asymptotic wave packet $\Phi(r,R,\theta,t_f)$ is projected out onto the states describing the products H+Ar–Br(ν,j) for different excitation energies of the parent cluster. The wave packet projection procedure has been described in detail in Ref. 18(a), and here we review it briefly. The states describing two separating H and Ar–Br(ν,j) fragments can be rigorously defined in the Jacobian coordinates (R',r',θ'), where

R' is the distance between H and the Ar–Br center-of-mass, r' is the Ar–Br separation, and θ' is the angle between the vectors $\mathbf{R}'$ and $\mathbf{r}'$. The angle $\theta'=0$ corresponds to the collinear configuration Ar–H–Br, with the H-position vector pointing towards the Ar atom. For a given excitation energy E of Ar–HBr, the above states are expressed as (within a time-dependent phase factor)

$$\xi^{(E)}_{\epsilon_k,v,j}(R',r',\theta')=\left(\frac{\mu_{R'}}{2\pi k_{R'}\hbar^2}\right)^{1/2} e^{ik_{R'}R'}\varphi^{(j)}_v(r') \times P_j(\cos\theta'), \quad (1)$$

where ϵ_k is the kinetic energy associated with the relative translational motion between the two fragments $[k_{R'}=(2\mu_{R'}\epsilon_k)^{1/2}/\hbar]$, $P_j(\cos\theta')$ is a normalized Legendre polynomial, and $\varphi^{(j)}_v(r')$ is a vibrational eigenstate of the Ar–Br stretch mode for a given j rotational state, with associated energy $E_{v,j}$. In the asymptotic limit the total energy of the fragments is expressed as $E=\epsilon_k+E_{v,j}$. A Jacobi transformation allows one to transform the $\xi^{(E)}_{\epsilon_k,v,j}(R',r',\theta')$ states into the $\eta^{(E)}_{\epsilon_k,v,j}(r,R,\theta)$ states, which are represented in the same Jacobian coordinates as the asymptotic wave packet. Now, the wave packet $\Phi(r,R,\theta,t_f)$ is projected out onto the $\eta^{(E)}_{\epsilon_k,v,j}(r,R,\theta)$ states

$$c_{v,j}(E)=\langle \eta^{(E)}_{\epsilon_k,v,j}(r,R,\theta)|\Phi(r,R,\theta,t_f)\rangle, \quad (2)$$

and from the projection amplitudes $c_{v,j}(E)$, probability distributions $P_{v,j}(E)=|c_{v,j}(E)|^2$ of Ar–HBr photodissociation into an atomic H fragment and an Ar–Br radical fragment in a rovibrational state (v,j), are obtained.

For the Ar–Br radical complex 424 (v,j) rovibrational states were found, including bound and quasibound ones, with $v_{\max}=11$ and $j_{\max}=74$. Out of these 424 states, 315 are bound states found for $j\leqslant 51$, and the remaining 109 ones are quasibound states supported by the centrifugal barrier. The quasibound states are very long-lived ones, and can be considered as bound states in practice regarding the time scale of hydrogen dissociation. Thus, for a given energy E the asymptotic wave packet is projected out onto 424 degenerate $\eta^{(E)}_{\epsilon_k,v,j}(r,R,\theta)$ states. Projections were performed for 20 different energies in the range of the Ar–HBr$(v=1)$ absorption spectrum, $E=1.5$–5.8 eV, for the two initial states of the cluster. The projection quadratures [Eq. (2)] were carried out in the original grid of the asymptotic wave packet. Convergence of these quadratures was checked in all the range of energies E investigated, by increasing the number of grid points and interpolating the asymptotic wave packet following the procedure described in Ref. 18(b). The quadratures were found to be converged with the original grid in the whole energy range. In order to ensure that the wave packet $\Phi(r,R,\theta,t_f)$ which is projected out is actually asymptotic, only the wave packet components corresponding to distances $r>19.9$ a.u. have been included in Eq. (2). Nonasymptotic components with $r<19.9$ a.u. correspond to the TF pathway, and do not affect the amplitudes $c_{v,j}(E)$.[26]

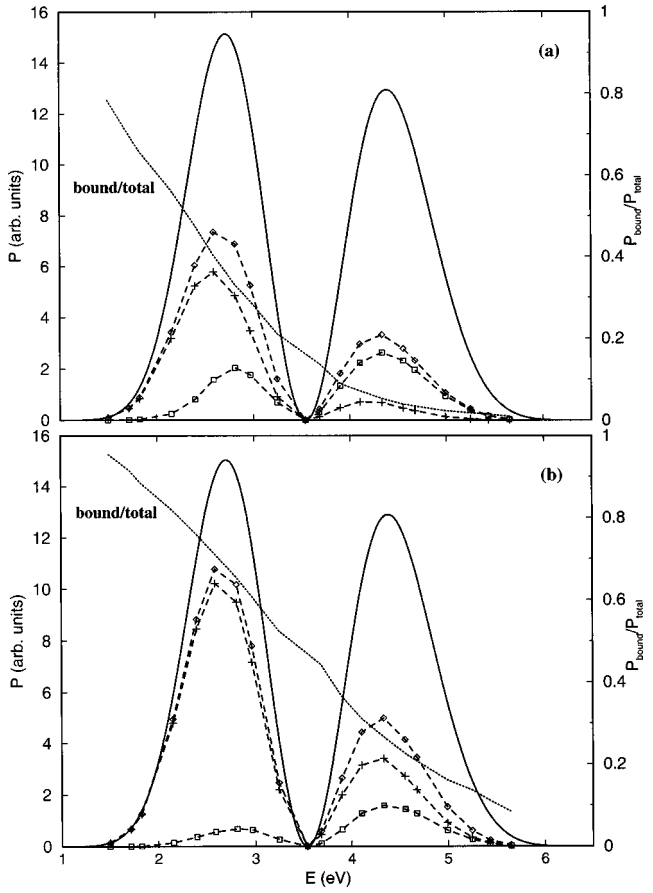

FIG. 1. Total probability of Ar–HBr$(v=1)$ photodissociation (solid line), probability of Ar–Br radical products ($\diamond$), partial probabilities of Ar–Br formation in bound states ($+$), and in quasibound states ($\square$), and ratio between the probability of Ar–Br in bound states and the total probability, $P_{\text{bound}}/P_{\text{total}}$ (dotted line) vs the initial excitation energy of the parent cluster. The two panels show results for the initial ground (a) and first excited (b) vdW states of Ar–HBr$(v=1)$. The limit $E=0$ corresponds to three separated atoms.

III. RESULTS AND DISCUSSION

A. Probability of Ar–Br formation

The probability of Ar–Br radical formation is shown in Fig. 1, along with the total probability of Ar–HBr$(v=1)$ photodissociation (related to the cluster absorption spectrum). The shape of the total probability distribution, with a node at medium energies, reflects the shape of the $v=1$ initial vibrational wave function of HBr. The partial probabilities of Ar–Br formed in bound and quasibound rovibrational states are also displayed in the figure. The percentage of Ar–Br radicals produced is obtained by dividing the probability of Ar–Br formation, $P_{\text{Ar–Br}}(E)$, by the total probability of cluster photodissociation, $P_{\text{total}}(E)$. The fraction of Ar–Br radicals formed in bound states is also shown in Fig. 1. For the two initial vdW states of Ar–HBr$(v=1)$ the probability of Ar–Br products is high (with respect to the total probability of photodissociation) in the whole range of energies E investigated. For the ground vdW state, the Ar–Br radical is produced dominantly in bound states for $E<3.5$ eV, while for $E>3.5$ eV the radical is formed mainly in quasibound states. By contrast, in the case of the excited

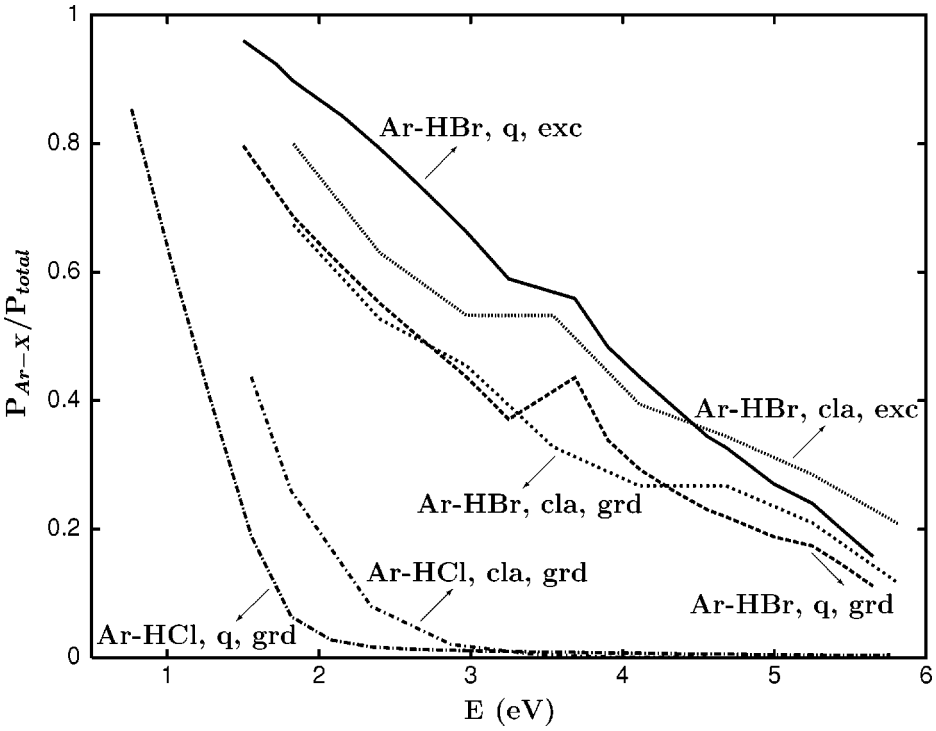

FIG. 2. Ratio between the probability of Ar–X products in bound and quasibound states, $P_{\mathrm{Ar-X}}$ (X=Br,Cl), and the total probability of Ar–HX photodissociation, P_{total} vs E. The ratios calculated quantum mechanically (q) and quasiclassically (cla) for the initial ground (grd) and first excited (exc) vdW states of Ar–HBr($v=1$), and the ground vdW state of Ar–HCl($v=0$) (Refs. 18 and 19) are shown.

vdW state the radicals are formed dominantly in bound rovibrational states (i.e., they are stable species) in all the energy range. The fraction of bound Ar–Br radicals found for the two cluster initial states displays strong differences, which increase with E. As we shall see below, this behavior is the consequence of a different fragmentation dynamics due to the different initial distribution of intracluster geometries.

The ratio $P_{\mathrm{Ar-Br}}(E)/P_{\mathrm{total}}(E)$ including the probability of Ar–Br formation both in bound and quasibound states is shown in Fig. 2 for the two initial states of Ar–HBr($v=1$). The difference between the Ar–Br fractions is now smaller than in Fig. 1, due to the higher population of Ar–Br quasibound states in the case of the initial ground vdW state of the cluster. For the sake of comparison, the previous quasiclassical and quantum mechanical results for the yield of Ar–Br[21] and Ar–Cl (Ref. 19) are also displayed. A good qualitative agreement is found between the quantum mechanical and quasiclassical yields of Ar–Br formation for the two initial states of the parent cluster. This agreement is fairly good in the case of the ground vdW state. Only for energies $E<3$ eV are there somewhat larger differences between the quantum and classical yields in the case of the first excited vdW state.

The present quantum mechanical simulations confirm the two main results found previously.[21] One such result is that the probability of Ar–Br formation is substantially higher for the excited vdW state, as a consequence that the initial distribution of intracluster angular geometries allows the H fragment to recoil freely, avoiding the collision with the Ar obstacle. Actually, the current results predict an even larger difference in the yield of Ar–Br produced from the two initial states (at least for $E<3$ eV), than the quasiclassical simulations. The other result is that radical formation is far more likely for Ar–HBr than for Ar–HCl photolysis (see Fig. 2), even when the initial angular distributions of the two clusters are very similar, as in the case of the ground vdW states of Ar–HBr($v=1$) and Ar–HCl($v=0$).

Quantum interference effects between the PF and the TF pathways played an important role in determining, and more specifically, in decreasing the yield of Ar–Cl formation.[19] Such effects are induced by the first collision of the recoiling hydrogen with Ar. Thus, possible interference effects in the Ar–HBr($v=1$) photolysis are expected to manifest mainly in the case of the initial ground vdW state, since the angular distribution of this state makes more likely the H/Ar collisions. However, good agreement is found between the quantum and classical predictions of the Ar–Br yield for the ground vdW state. The discrepancies observed for the excited vdW state (for $E<3$ eV) could be due to quantum effects, but also to methodological differences between the quantum-mechanical and quasiclassical simulations (e.g., initial state representation, final analysis of the product distributions).

B. Ar–Br product state distributions

Rovibrational state distributions, $P_{v,j}(E)$, of the Ar–Br fragment produced when photolysis starts from the ground and first excited vdW state are shown in Figs. 3 and 4, respectively, for several excitation energies. A surprisingly good agreement is found between the quantum-mechanical and quasiclassical rovibrational distributions for the two initial states of Ar–HBr($v=1$). By summing the $P_{v,j}(E)$ distributions over v or j, rotational and vibrational distributions, respectively, are obtained. For both the rotational (shown in Fig. 5) and the vibrational (not shown here) distributions, again very good agreement with the corresponding quasiclassical distributions is observed.

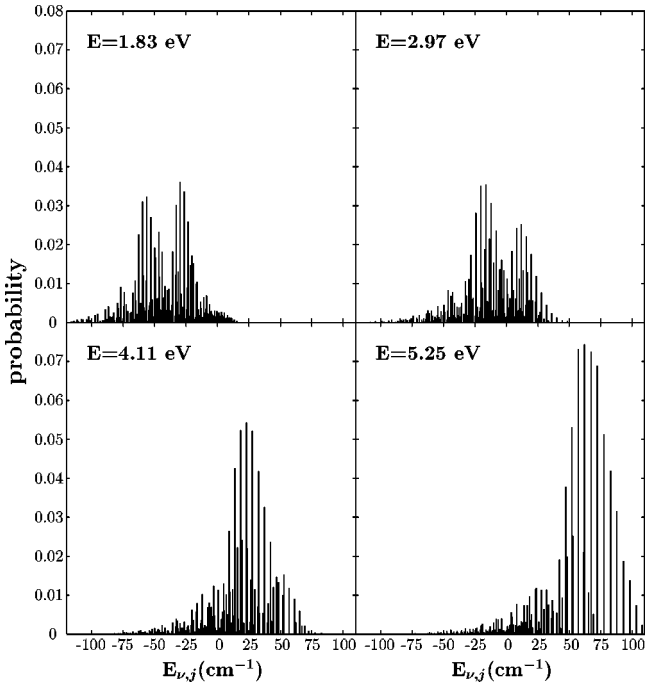

FIG. 3. Rovibrational state distributions of the Ar–Br radical fragment for four different excitation energies, when photolysis starts from the ground vdW state of Ar–HBr($v=1$). Negative and positive $E_{v,j}$ energies correspond to bound and quasibound rovibrational states of Ar–Br, respectively. All the distributions are normalized to unity.

The main difference between the distributions of Fig. 3 and 4 is that the Ar–Br fragments are clearly more excited when they are produced from the initial ground vdW state of Ar–HBr($v=1$). For the same excitation energy, the distributions of the excited vdW state exhibit a substantially higher population in the Ar–Br bound states. The higher excitation of the distributions of Fig. 3 is essentially due to a higher

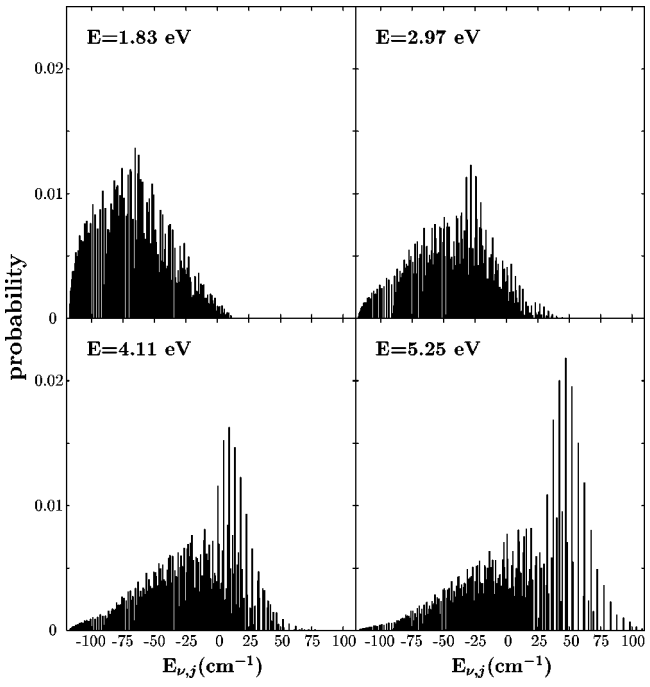

FIG. 4. Same as Fig. 3 for the first excited vdW state of Ar–HBr($v=1$).

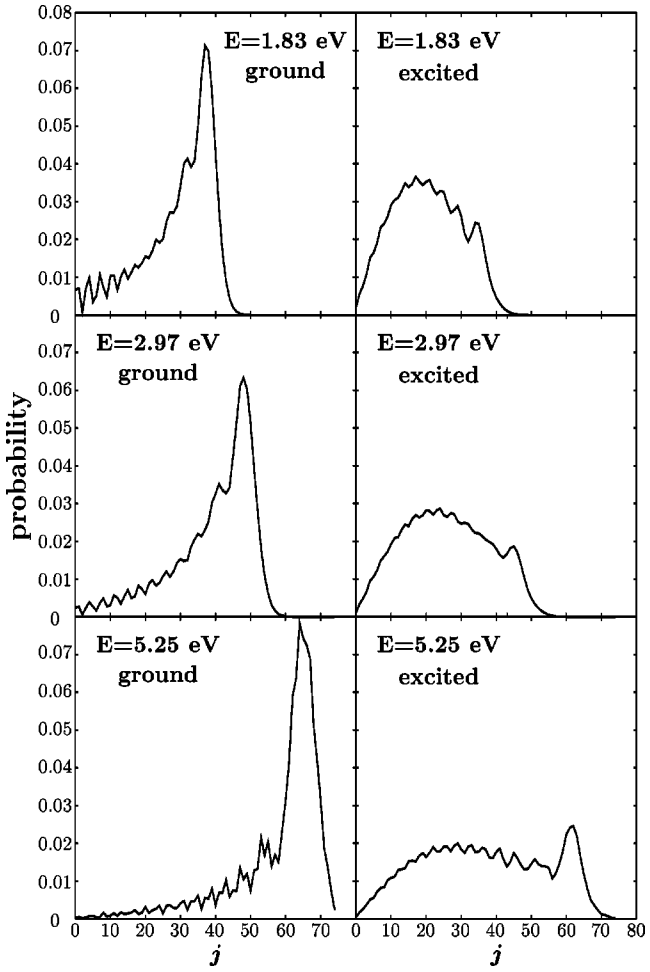

FIG. 5. Rotational distributions of Ar–Br for three excitation energies, starting from the ground and first excited vdW state of Ar–HBr($v=1$). All the distributions are normalized to unity.

rotational excitation, as can be seen from the rotational distributions of Fig. 5. When the hydrogen recoils it produces a torque on the radical fragment. For the hydrogen initial orientations corresponding to the distribution of the ground vdW state this torque is larger, causing a higher rotational excitation of Ar–Br than for those associated with the excited vdW state distribution.

Comparison of the quantum and classical results for Ar–Br formation indicates that quantum interference effects are clearly less intense in Ar–HBr than in Ar–HCl. In particular, the Ar–Br rotational distributions corresponding to the ground vdW state of Ar–HBr($v=1$) (left panels of Fig. 5) exhibit a relatively weak structure, as compared with the pronounced pattern of peaks found in the rotational distributions of Ar–Cl.[18(b),19] Such results raise some intriguing questions. One of them is why interference effects manifest in Ar–HCl more strongly than in Ar–HBr, despite the similarity in the initial ground vdW states of both clusters, and that the excited electronic potential surfaces are not so different. Another question is related to the large difference in the yield of Ar–Cl and Ar–Br formation. Indeed, a factor which contributes to this difference is that for Ar–Cl there is a larger amount of energy available than for Ar–Br (for the same cluster excess energy E), due to the different H/Cl and

H/Br mass ratios. In light of the present results, however, one may ask whether this is the only reason, or is there a relation between the radical yield and the intensity of interference effects. In the following we shall analyze these points.

For a given excess energy E there is a factor ~ 2.2 between the amounts of energy available for Ar–Cl and Ar–Br. In addition, the lowest bound and highest quasibound energy levels of Ar–Br are 117.6 cm^{-1} below and 108.1 cm^{-1} above the dissociation limit of the Ar–Br potential, respectively, while in the case of Ar–Cl these energy levels are 104.0 cm^{-1} below and 99.8 cm^{-1} above the dissociation limit, repectively. This means that Ar–Br can accommodate 1.1, times more energy available as internal energy than Ar–Cl. Thus, assuming that the partition of the available energy among the radical internal (rovibrational) and center-of-mass translational energy is roughly similar for both Ar–Br and Ar–Cl, the effect of the energy available in decreasing the yield of radical formation is $2.2 \times 1.1 = 2.4$ times smaller in Ar–Br than in Ar–Cl. However, Fig. 2 shows that for the initial ground vdW states of Ar–HBr($v=1$) and Ar–HCl($v=0$), the yield of Ar–Br products is much higher than 2.4 times the yield of Ar–Cl, for all energies E.

In addition to the effect of the available energy, the yield of radical products is also determined by the probability of the first collision between the recoiling hydrogen and the Ar obstacle, as discussed above for the Ar–HBr($v=1$) photolysis from the excited vdW state. A higher probability of this collision implies a lower radical yield, as well as stronger manifestations of quantum interference effects in the radical product distributions. Inspection of the wave packet dynamics for the initial ground vdW state shows that the H/Ar collision is less likely in the Ar–HBr($v=1$) photolysis than in the Ar–HCl($v=0$) case. This is reflected in the H fragment angular distributions obtained from Ar–HBr($v=1$) photodissociation through the PF pathway (Fig. 6). Such distributions display most of their intensity at relatively low and medium angles, and only a slow shift from low to medium angles is observed with increasing E. This behavior contrasts with that of the corresponding angular distributions of Ar–HCl($v=0$), where the intensity at medium and low angles vanished rapidly with E, consistently with a higher probability of a H/Ar collision. Thus, the lower probability of the H/Ar collision in the Ar–HBr($v=1$) photolysis from the ground vdW state would explain that the Ar–Br yield is remarkably higher than 2.4 times the Ar–Cl yield, and that interference manifestations are less intense in the Ar–Br distributions as compared with the Ar–Cl ones.

The result that the H/Ar collision is less likely in Ar–HBr($v=1$) than in Ar–HCl($v=0$) can be understood in terms of geometrical features of the initial ground vdW states of the two clusters. On the one side, although the two initial angular distributions are similar, that of Ar–HBr($v=1$) is somewhat shifted towards higher angles, involving less blockage of the hydrogen. Specifically, the maximum of the Ar–HBr($v=1$) distribution is at $\theta = 33.6°$, while that of the Ar–HCl($v=0$) distribution is at $\theta = 30.8°$, and the Ar–HBr ($v=1$) distribution exhibits more population at very high angles (see Fig. 1 of Ref. 21). On the other side, for the ground vdW state the equilibrium distances between Ar and the center of mass of HBr and HCl are 4.28 and 3.99 Å, respectively. In order to reach the same excess energy E in the repulsive $A\,^1\Pi$ potential, the H–Br distance is typically 0.14 Å larger than the H–Cl one. This implies that the initial distance between the H and Ar atoms is larger in Ar–HBr($v=1$) than in Ar–HCl($v=0$), and then a hydrogen recoiling with a similar energy and orientation is more likely to avoid a collision with Ar in the case of Ar–HBr($v=1$). The combined effect of the two above-mentioned geometrical features of the cluster initial state yields a lower probability of the H/Ar collision in the Ar–HBr($v=1$) photolysis, as compared with Ar–HCl($v=0$).

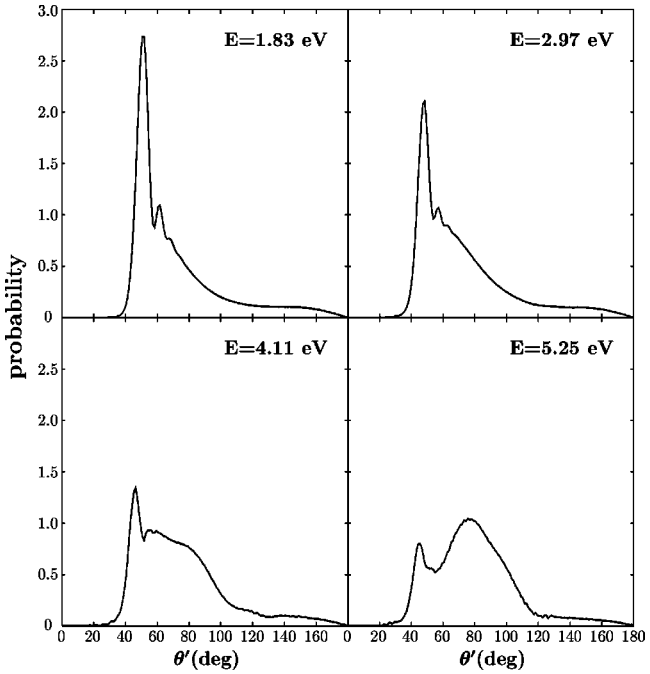

FIG. 6. Angular distributions of the H fragment produced by partial fragmentation of Ar–HBr($v=1$) from the initial ground vdW state, for four excess energies of the cluster. The $\sin\theta'$ factor is included in the distributions. All the distributions are normalized to unity.

Some predictions and trends can be suggested for clusters of the Ar–HX (X=F,Cl, Br,I) family based on the above discussion. The amount of energy available for the Ar–X radical increases (for the same energy E) when going from X=I to X=F, and the Ar–X product yield will decrease correspondingly. For a cluster initial state associated with the Ar–H–X isomer, when X goes from I to F the initial angular distribution becomes gradually more concentrated at low angles,[22] and the distance between Ar and the HX center of mass becomes smaller. The expected result is an increase of the H/Ar collision probability, and consequently a decrease of the Ar–X yield and an increase of manifestations of interference effects in the product distributions. By preparing an initial angular distribution of the cluster corresponding to the Ar–X–H isomer, the effect of the H/Ar collision is significantly reduced, as shown in this work. More generally speaking, the probability of the H/Ar collision, and therefore the radical product yield, can be controlled through the shape of the cluster state initially prepared, which determines the initial orientation and distance of the hydrogen with respect to

the Ar obstacle. In this sense, the possibility to reduce the collision probability by increasing the initial H–Ar distance, through excitation of the vdW stretching mode, should also merit attention.

IV. CONCLUSIONS

Wave packet dynamics simulations of the UV photolysis of Ar–HBr($v=1$) are reported. Cluster photolysis is started from two different initial states. One of them is the ground vdW state of Ar–HBr($v=1$), for which the equilibrium geometry corresponds to the Ar–H–Br isomer. The other state is the first excited vdW state of Ar–HBr($v=1$), associated with the equilibrium geometry of the Ar–Br–H isomer. The present quantum-mechanical results are compared to previous quasiclassical simulations of the photolysis for the two initial states, and good agreement is found. This agreement confirms the two main conclusions of the earlier quasiclassical work. One such conclusion is that the yield of Ar–Br radical products is substantially higher for the initial distribution of hydrogen orientations associated with the excited vdW state of the cluster. This is a consequence that for this initial state a collision of the recoiling hydrogen with the Ar obstacle is less likely, which increases the probability of radical survival. The other conclusion is that the probability of radical complex formation is much higher for Ar–HBr($v=1$) photolysis than for the previously studied Ar–HCl($v=0$) photolysis, even for the initial ground vdW states of the two clusters, which are similar in shape. The smaller amount of energy available for the Ar–Br fragment does not account for the large difference between the Ar–Br and Ar–Cl yields.

The current wave packet simulations predict that strong quantum effects are not present in the Ar–HBr($v=1$) photolysis, for the two initial states. In the case of the initial ground vdW state of Ar–HBr($v=1$) this finding is again in sharp contrast with the previous results of Ar–HCl($v=0$) photolysis. The lower probability of a collision between the recoiling hydrogen and the Ar atom is also suggested here to explain both the higher Ar–Br yield and the less intense interference manifestations for Ar–HBr($v=1$) photolysis from the ground vdW state, as compared with the Ar–HCl ($v=0$) case. Geometrical differences between the ground vdW states of Ar–HBr($v=1$) and Ar–HCl($v=0$) would be responsible for the lower H/Ar collision probability in the Ar–HBr($v=1$) photolysis. More specifically, the angular distribution is somewhat shifted towards higher angles and the distance between H and Ar is typically larger in the Ar–HBr($v=1$) initial state.

Finally, it is shown that the probability of the H/obstacle collision, which affects greatly the radical product yield, depends to a large extent on the geometrical features of the cluster initial state. Thus, selecting the shape of the cluster state initially prepared appears as a promising venue to control the probability of this collision, and then of the yield of the photolysis products. It should be very interesting to investigate the effect of these geometrical features in the photolysis of Ar–HX clusters different than Ar–HCl and Ar–HBr, as well as of more complicated precursor clusters, like Ar–H_2S, Ar–H_2O, and $(HX)_2$.

Note added in proof. Two other theoretical studies (Refs. 27 and 28) on the photodissociation of ArHBr were submitted at about the same time we submitted the present work.

ACKNOWLEDGMENTS

This work was supported by C.I.C.Y.T. (Ministerio de Ciencia y Tegnología), Spain, Grant No. BFM-2001-2179, and by the European network TMR, Grant No. HPRN-CT-1999-00005.

[1] J. Segall, Y. Wen, R. Singer, C. Wittig, A. García-Vela, and R. B. Gerber, Chem. Phys. Lett. **207**, 504 (1993).
[2] C. Jaques, L. Valachovic, S. Ionov, Y. Wen, E. Böhmer, J. Segall, and C. Wittig, J. Chem. Soc., Faraday Trans. **89**, 1419 (1993).
[3] J. Zhang, M. Dulligan, J. Segall, Y. Wen, and C. Wittig, J. Phys. Chem. **99**, 13680 (1995).
[4] K. Liu, A. Kolessov, J. W. Partin, I. Bezel, and C. Wittig, Chem. Phys. Lett. **299**, 374 (1999).
[5] M. A. Young, J. Chem. Phys. **102**, 7925 (1995).
[6] D. F. Plusquellic, O. Votava, and D. J. Nesbitt, J. Chem. Phys. **101**, 6356 (1994).
[7] O. Votava, D. F. Plusquellic, T. L. Myers, and D. J. Nesbitt, J. Chem. Phys. **112**, 7449 (2000).
[8] S. R. Mackenzie, O. Votava, J. R. Fair, and D. J. Nesbitt, J. Chem. Phys. **105**, 11360 (1996); **110**, 5149 (1999).
[9] R. Baumfalk, U. Buck, C. Frischkorn, N. H. Nahler, and L. Hüwel, J. Chem. Phys. **111**, 2595 (1999).
[10] C. A. Picconatto, H. Ni, A. Srivastava, and J. J. Valentini, J. Chem. Phys. **114**, 7073 (2001).
[11] R. Alimi and R. B. Gerber, Phys. Rev. Lett. **64**, 1453 (1990).
[12] A. García-Vela, R. B. Gerber, and J. J. Valentini, Chem. Phys. Lett. **186**, 223 (1991); J. Chem. Phys. **97**, 3297 (1992).
[13] A. B. McCoy, Y. Hurwitz, and R. B. Gerber, J. Phys. Chem. **97**, 12516 (1993).
[14] T. Schröder, R. Schinke, and Z. Bačić, Chem. Phys. Lett. **235**, 316 (1995).
[15] K. M. Christoffel and J. M. Bowman, J. Chem. Phys. **104**, 8348 (1996).
[16] E. Narevicius and N. Moiseyev, Chem. Phys. Lett. **287**, 250 (1998).
[17] A. García-Vela, J. Chem. Phys. **108**, 5755 (1998).
[18] J. C. Juanes-Marcos and A. García-Vela, J. Chem. Phys. **112**, 4983 (2000); (b) **115**, 5692 (2001)(E).
[19] J. C. Juanes-Marcos and A. García-Vela, J. Phys. Chem. A **106**, 236 (2002).
[20] J. R. Fair and D. J. Nesbitt, J. Chem. Phys. **113**, 10962 (2000).
[21] R. Prosmiti and A. García-Vela, J. Chem. Phys. **117**, 100 (2002).
[22] R. Prosmiti and A. García-Vela, Chem. Phys. Lett. **366**, 238 (2002).
[23] In this work and in Ref. 21 the Ar–Br potential in the excited electronic state was taken from Y. Zhao *et al.* J. Chem. Phys. **101**, 6538 (1994). By mistake, in Ref. 21 the Ar–Br potential of P. Casavecchia *et al.*, **75**, 710 (1981) was referenced. Actually the two potentials have the same functional form, and even the same or slightly different values for the parameters.
[24] H. Tal-Ezer and R. Kosloff, J. Chem. Phys. **81**, 3967 (1984).
[25] H. Guo, J. Chem. Phys. **96**, 6629 (1992).
[26] J. C. Juanes-Marcos and A. García-Vela, J. Chem. Phys. **111**, 2606 (1999).
[27] B. Leptit and D. Lemoine, J. Chem. Phys. **117**, 8676 (2002).
[28] J. Trin, M. Monnerville, B. Pouilly, and H.-D. Meyer, J. Chem. Phys. **118**, 600 (2003).